Available online at www.sciencedirect.com

ScienceDirect

Procedia CIRP 108 (2022) 88–93

www.elsevier.com/locate/procedia

6th CIRP Conference on Surface Integrity

Support Structure Impact in Laser-Based Powder Bed Fusion of AlSi10Mg

Marc Schmidt[a]*, Sebastian Greco[a], Daniel Müller[a], Benjamin Kirsch[a], Jan C. Aurich[a]

[a]*Institute for Manufacturing Technology and Production Systems, TU Kaiserslautern, 67663 Kaiserslautern, Germany*

* Corresponding author. Tel.: +49-631-205-5483; fax: +49-631-205-3238. *E-mail address:* marc.schmidt@mv.uni-kl.de

Abstract

Laser-Based Powder Bed Fusion (L-PBF) is one of the most established additive manufacturing methods used to build metallic components. During L-PBF, cross-sections of the components are melted in a powder bed by a laser. To connect the workpieces to the building platform, to dissipate the heat induced by the laser and to reduce characteristic distortion, support structures are applied. So far, different support structures were mostly compared with each other with regard to the resulting process results, such as microstructure, residual stresses and distortion. In this study, however, the influence of the area supported by the support structures is systematically investigated. For two different supports (columns and meanders), the percentage of the supported area is varied between 0 and 70% and the influences on the microhardness profiles, melt path geometries and distortion are analyzed. For instance, by increasing the supported area, it has been possible to reduce distortion by up to approximately 30%.

Keywords: additive manufacturing; support structures; material properties; distortion; residual stresses

1. Introduction

Additive manufacturing processes enable a much higher freedom of design for technical components compared to traditional manufacturing processes. This is realized through the layer-by-layer generation of the workpiece structure, which enables the production of highly complex and functionally integrated components [1]. Laser Powder Bed Fusion (L-PBF) is one of the most widely used additive manufacturing processes for metallic materials. In this process, fine-grained metallic powders are selectively melted, and thin layers are created by overlapping the welding tracks. During the melting process of the powder material and the subsequent solidification, very high local temperature gradients of up to 10^7 K/s occur [2]. These lead to elasto-plastic strains and compressions in the individual layers. The differences in material properties at different temperatures lead to residual stresses in the heat-affected zone (HAZ) due to an inhomogeneous temperature field. The molten material experiences positive thermal strain, which leads to compression of the surrounding colder material and results in plastic deformation [3]. As the melt cools, tensile stresses develop due to the yielding behavior of the material while the plastic strains remain in the HAZ. The underlying effect is called the temperature gradient effect (TGE). The extent of plastic deformation per layer significantly depends on the component stiffness and the temperature gradients [4].

One way of reducing residual stresses and distortion is to preheat the build plate. For 316L stainless steel and the titanium alloy Ti6Al4V, a positive influence of preheating the build plate has already been demonstrated [3, 5]. Buchbinder et al. [4, 6] investigated the reduction of distortion for AlSi10Mg by preheating the build platform using a cantilever specimen geometry. For this purpose, the preheating temperature was varied between 100 °C and 250 °C in 50 °C steps. It was observed that above a preheating temperature of 150 °C, the distortion began to decrease significantly. Above 200 °C, no more distortion could be detected within the measurement accuracy. The hardness of the material stayed at a constant level of 130-140 HV0.1 up to a temperature of 150 °C. Above this preheating temperature, it began to decrease significantly

2212-8271
10.1016/j.procir.2022.03.019

to a value of 90 HV0.1 at 250 °C. The cause for this is the grain coarsening associated with the high temperature, in particular the exceeding of the critical size of the intermetallic Mg_2Si phase.

The additively manufactured components are not manufactured directly on the building platform but are connected to the building platform via support structures. These are needed for the fabrication of overhanging structures as well as for mechanical and thermal reasons. Thus, the support structures are also used in other additive manufacturing processes, such as material extrusion and stereolithography, to realize overhangs and create complex 3D structures. In these processes, the support structures can also consist of other materials and can be dissolved or washed out after manufacturing, for example [7]. In the case of L-PBF, the supports are built from the same powder material.

The surrounding powder has a much lower thermal conductivity, so heat is dissipated mainly through already solidified material via the build platform and against the build direction. Unconnected areas and overhangs therefore tend to overheat and exhibit significantly lower cooling rates due to heat accumulation. Therefore, the addition of support structures at such locations is often mandatory. These are created together with the component from the powder bed.

A frequently used support structure is the block structure with tooth-shaped contact surface to the supported workpiece. In various studies [8, 9] the influence of the tooth geometry and consequently of the contact area on overhang areas and the sample's down-facing surface was investigated experimentally and simulatively. It was found that with increasing tooth contact area, the residual stresses of overhang structures could be reduced. Furthermore, by reducing the spacing and height of the block supports, their mechanical strength could be increased to resist peel failure. In addition, density of supports was found to be a key factor in reducing residual stresses.

In general, there are only few systematic experimental studies on variations and different geometry parameters of support structures. Therefore, the subject of this research is the investigation of two commonly used support structures (column and meander supports) under variation of the supported area.

2. Methods

2.1. Additive Manufacturing

T-shaped cantilevers were manufactured additively using L-PBF. The cantilevers' geometry is equal to the geometry used in [4] and is particularly sensitive to the identification of distortion. The cantilevers consist of a ridge with a symmetrical bar attached above. The down-facing surfaces of this bar were supported. To analyse the support structure's impact, two different types of support structures (columnar and meander) were used, and the percentage of supported area was varied. The geometric dimensions and a schematic representation of the support structure types are shown in Figure 1.

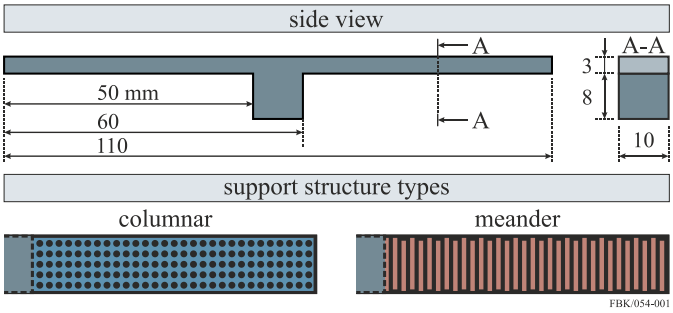

Fig. 1. Sample geometry of the twin cantilever and the different support structure types used.

For both support structure types, 10-70 % of the down-facing surface of the cantilever was supported in each case. Support areas of only up to 70 % were possible, as the adjacent columnar support structures came into contact above this percentage value. All support structures were distributed equidistantly. The additive manufacturing system ProX DMP 320 by 3D Systems* was used for L-PBF. This system is equipped with a 500 W fiber laser (λ = 1070 nm, 65 µm laser spot diameter) and a 275 x 275 x 380 mm building volume. AlSi10Mg powder with an average powder particle size of d_{50} = 49 µm (d_{10} = 32 µm, d_{90} = 75 µm) was applied. The particle size was measured with the powder characterization unit Bettersizer S3 Plus by 3P Instruments*. During L-PBF, an inert atmosphere (O_2 < 100 ppm) was provided by argon. The building platform was not heated. The process parameters of L-PBF differ in dependence to the melted volume.

Table 1. L-PBF process parameters

parameter	component	support
laser power	300 W	325 W
scanning speed	1400 mm/s	1400 mm/s
layer thickness	30 µm	60 µm
hatch distance	100 µm	100 µm

Thus, different process parameters are used for component and support volumes, which can be seen in Table 1. Each combination of support structure type and percentage of supported surface was additively manufactured eight times. Of these, four samples were heat treated each (stress relief annealing). The heat treatment was performed at a heating rate of 1 °C/min up to a temperature of 300 °C with a dwell time of 2 h. In the following, the specimens are named with respect to the support structure type (C for columns, M for meanders) and the percentage of the supported area (10-70 %). The stress relieved specimens are additionally given the abbreviation HT for heat treated.

2.2. Distortion Measurement

A 3D coordinate measuring device, TESA* micro-hite 3D DCC1, was used to determine the distortion of the twin cantilever in z-direction. The measurement scheme is given in Figure 2.

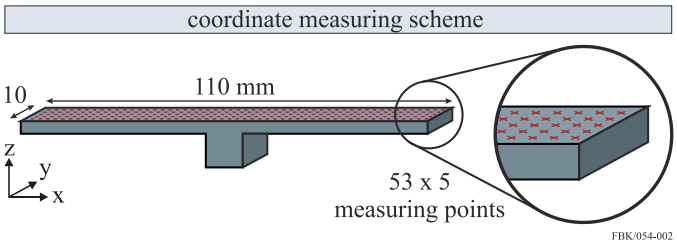

Fig. 2. Scheme of the coordinate measurements for determining the distortion.

The measurement scheme consisted of 53 measuring lines in y-direction, each with 5 measurement points. The outer measuring points had a distance of 3 mm in x-direction and 0.2 mm in y-direction to the contour of the twin cantilever. The distance between the measuring points was chosen to be 2 mm in x-direction and 2.4 mm in y-direction. To ensure sufficient statistical validation, four heat treated and four as built twin cantilevers were evaluated for each type of support structure. For the evaluation of the distortion, the 5 measuring points of each measuring line were averaged. Afterwards, averaging of the mean values of the lines was applied to the four components with identical support structure and heat treatment condition. In addition, an averaged standard deviation $\bar{\sigma}$ was calculated from all mean values of the four specimens with identical support structure and heat treatment condition. To identify possible torsion effects, contour plots were created using Matlab[1]. For this purpose, all 265 measuring points of a twin cantilever were imported, and the z-coordinates of all points were related to the mean z-coordinates value of measuring line 27 (center of the twin cantilever).

2.3. Microstructural Analysis

After the distortion measurements, the twin cantilever specimens were cut off from the building plate at the remaining joint by means of a band saw. To characterize the influence of the support structures on the microstructure, pieces of approximately 15 mm length were cut off at the bar ends of each sample type and subsequently sliced open. For this purpose, a Mecatome T210 precision cutting machine from Presi* was used. In the next step, the separated samples were warm embedded in a Mecapress 3 and metallographically prepared on a Mecatech 334 grinding and polishing machine from Presi*. The grinding and polishing procedures included plane grinding of the specimens with SiC abrasive paper up to a grit size of P1200 and polishing with diamond suspensions of 9 µm down to 0.05 µm grit size. To contrast the microstructure, the specimens were etched by immersion with 5 % sodium hydroxide solution for 10-15 s after polishing. Light microscopic images were taken with a BX41M from Olympus* and a DM6 from Leica*.

The microstructure of additively manufactured workpieces has a characteristic structure consisting of individual melt paths. Since these depend on the selected process parameters, their geometry was determined based on further etched cross sections. The etching for this purpose was done on polished samples by immersion etching for 15-20 s using Kroll etchant. The melt path height and width of a sample was measured on 25 melt paths from a total of 3 samples each. In total, 75 melt paths were measured for each sample condition.

2.4. Hardness Measurement

The hardness measurements were carried out on a MicroMet 5100 hardness tester from Buehler* according to DIN EN ISO 6507-1 [10]. A test load of F = 0.098 N (HV0.01) was selected to achieve good resolution in the edge region of the down-facing surface of the cantilever. The measurement scheme for the hardness indentations is shown in Figure 3. The hardness profiles were recorded starting from the top of the bar to the supported down-facing surface with decreasing intervals.

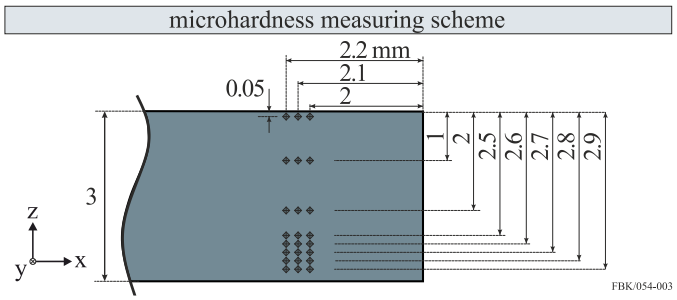

Fig. 3. Scheme of the microhardness indents in the sample cross section.

For statistical validation, 3 hardness indents of each distance were lined up next to each other. Measurements were taken to a depth of 2.9 mm, divided into 8 measured values, as the underside of the bar frayed depending on the supported area. In total, the hardness profiles from 3 samples of each condition were measured.

3. Results and Discussion

3.1. Distortion

In Figure 4 the distortions of the different combinations of support structure type, percentage of supported surface and heat treatment are shown for 10 %, 40 % and 70 % supported area. The remaining samples have been excluded from the plot for the purpose of clarity, however, they are proportionally positioned between the presented samples.

Regardless of the type of support structure, very similar levels of distortion were found for identically supported areas. An increase of the supported area led to a decrease of the component's distortion. An additional stress relieving heat treatment significantly reduced the distortion of the structures. The effect of heat treatment was observed independent from the type of support structure.

The influence of the amount of supported area is due to the temperature gradient effect. A higher percentage of supported area leads to more heat being dissipated into the building platform that acts as a heat sink in the L-PBF system and thus to lower temperatures in the molten volume. Lower temperatures reduce the temperature gradient effect and lead to less distortion. Since heat treatments reduce residual stresses, the distortion resulting from the temperature gradient effect is reduced. Therefore, the heat treatments seem to have a bigger

influence on the reduction of distortion than the support structures.

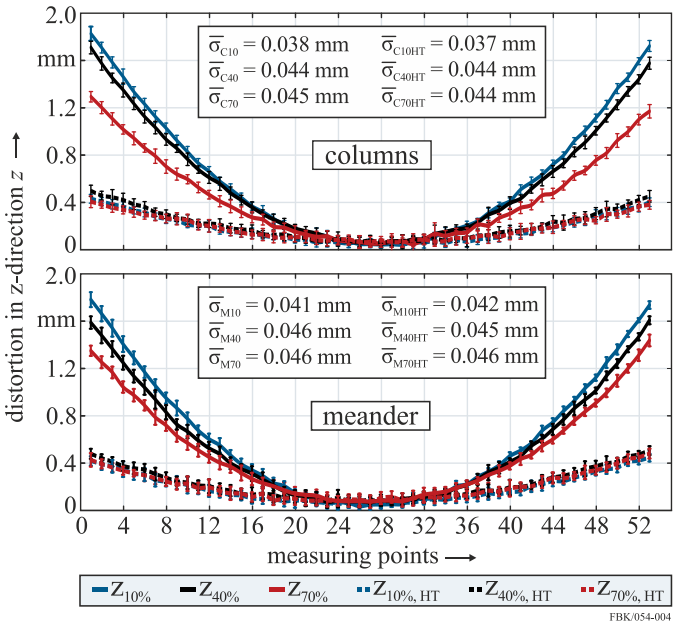

Fig. 4. Measurement of distortion over the bar length (x-direction). One measuring point represents the average of 5 values over the bar width (y-direction).

In Figure 5, colormaps of the distortion measurement are given, which allow information on possibly occurring torsion of the cantilevers.

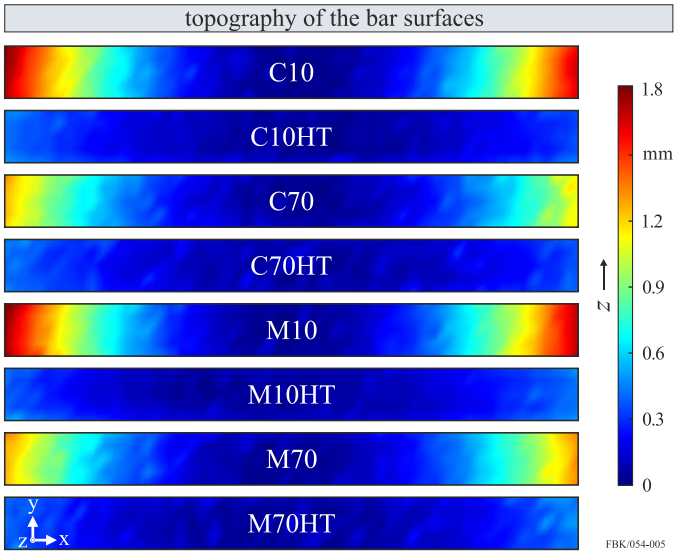

Fig. 5. Topographically colored illustration of the measured bar top surfaces to visualize the distortion.

No torsion of the bar at the cantilever's top was detected in any of the analysed specimens. Furthermore, the results from Figure 4 are confirmed, which illustrate a symmetrical distortion of the bar starting from the centre. The symmetry of the distortion in x- and y-direction is due to the equidistant distribution of the support structures leading to symmetrical thermal loads.

3.2. Microstructure

Light optical micrographs taken from the bulk material to analyse the melt path geometry are shown in Figure 6. Two specimens with columnar support structure for the extremes of 10 % and 70 % supported area are shown as examples. The evaluation of the melt path heights and widths showed the tendency that the melt track width increases with a percentage decrease in the supported area.

This can be explained by the fact that with less supported area, less heat can be dissipated from the process. Therefore, with the adjacent melt path, there is still more heat in the previous track and less energy is required to melt the new track. Consequently, the constant laser power results in the broadening of the melt paths as more energy is introduced into the system. The melt path heights and widths are listed in Table 2 for representative selected samples of different supported areas.

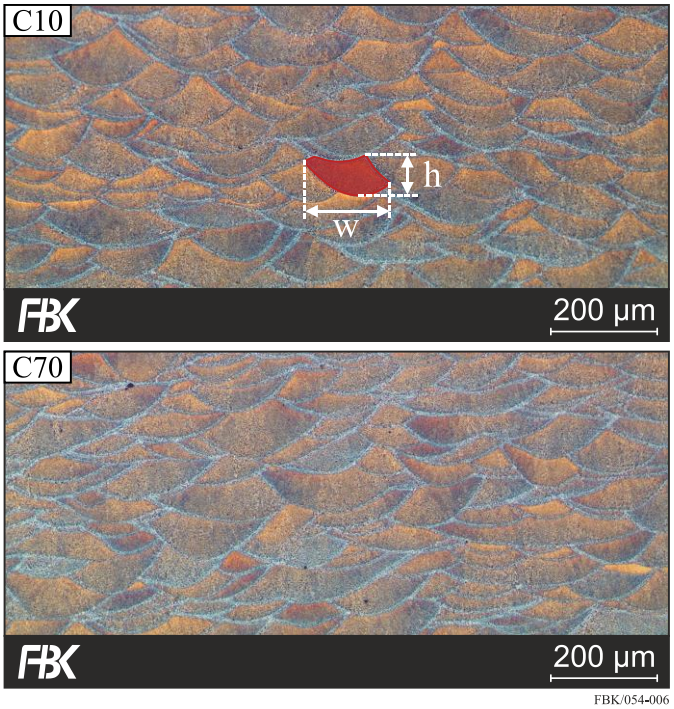

Fig. 6. Light optical micrographs of the specimens with columnar support structures with (a) 10% and (b) 70% supported area.

Table 2. Determined melt path geometries

Sample	Melt path height in µm	Melt path width in µm	Aspect ratio
C10 %	85 ± 14	199 ± 39	2.34 ± 0.84
C70 %	74 ±17	168 ± 30	2.26 ± 0.93
M10 %	80 ± 17	181 ± 34	2.26 ± 0.91
M70 %	81 ± 18	166 ± 32	2.06 ± 0.85

Furthermore, the transition area from the support structures to the actual component was examined based on micrographs.

Figure 7 shows etched cross sections for the columnar support structure type with 10 % supported area as an example. Dross defects can be seen above the support structure. In this region, the α-Al solid solutions and the cellular Al-Si eutectic around them are much coarser than in the melt paths of higher layers. These dross defects often occur at areas of poor heat dissipation such as the down-skin surfaces which are not supported but lie in the powder bed [11, 12]. Frequently, these areas therefore also bind only partially melted powder grains, which can be seen in the bottom right in Figure 7a. Since the powder has much poorer thermal conductivity, these areas remain molten longer. This results in a coarser microstructure since nucleation from the melt is more slowly.

The fact that these areas appear despite the support structure at this point shows that 10 % of the supported area still does not provide sufficient heat dissipation. In addition, pores are clearly visible in this zone. These arise at a critical energy input and lead to instable melt pools, which can form spherical pores [13].

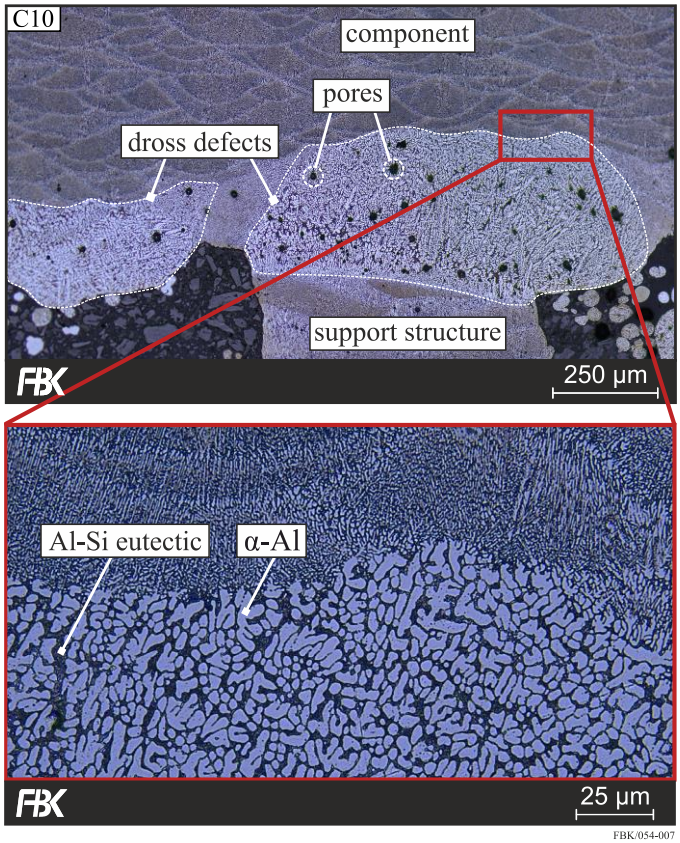

Fig. 7. Etched cross section of the as-built C10 sample showing an overview above the support structure and a detail view at the affected area.

In contrast, Figure 8 shows a sample with a columnar support structure and 70 % supported area. In this figure, the transition from the support structure to the component is almost seamless. The regular melt pool structure persists, and the melt pools of the support structures are only slightly higher due to the other process parameters.

The dross defects began to disappear from 50 % supported area above the support structures, so that above this area sufficient heat is dissipated from the process zone and the microstructure solidifies more finely grained and uniformly.

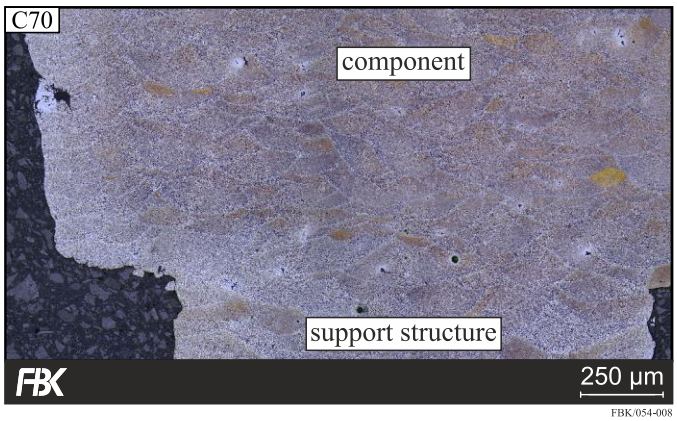

Fig. 8. Etched cross section of the as-built C70 sample above the support structure.

3.3. Hardness

The hardness measurements according to Vickers are shown in Figure 9 for both support structure types with 10 % and 70 % supported area in the as-built and stress-relieved condition, respectively. The hardness profile is shown from the top of the bar towards the support structures.

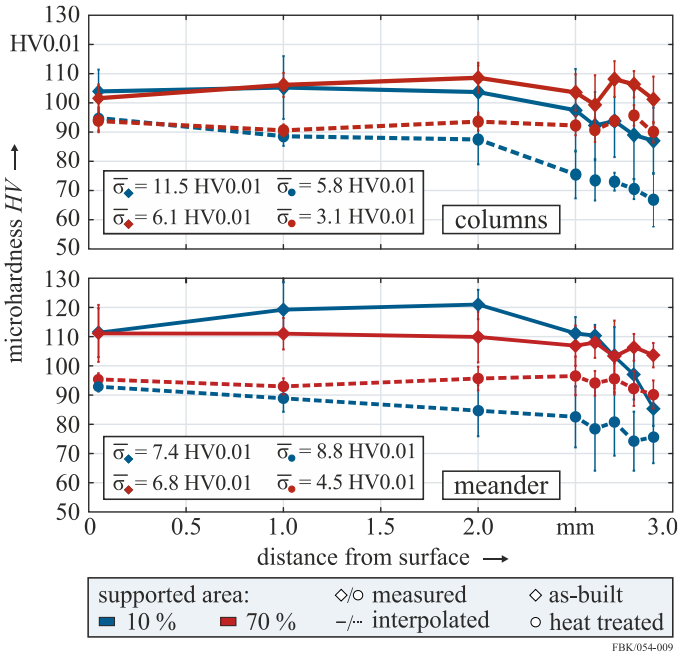

Fig. 9. Measured hardness profiles starting from the top of the bar.

The two as built and the two heat-treated specimen conditions with columnar support structures each show a largely constant hardness level in the bulk up to about 2.0 mm. From about 2.5 mm, the hardness starts to decrease non-steadily. In the C10 sample, this effect is much more pronounced, since the microstructure in the layers close to the support structure is coarser and packed with keyhole pores. This results from the higher temperatures in this sample and the associated dross defects. The sample C70 does not show a

noticeable drop in hardness in the area close to the support structure, in fact the hardness tends to increase slightly again from 2.7 mm. The same can be seen with the appropriately heat-treated sample C70HT, which allows the assumption that an equilibrium of the heat conduction and consequently a uniform microstructure development occurs from this distance onwards. In general, the as built and the heat-treated specimens show approximately the same profiles in different hardness regions. This is due to the heat treatment, which reduces residual stresses and lowers the hardness.

Similar observations can be made for the meander specimens. The hardness of specimens M10 and M10HT decreases steadily towards the support structure area. In contrast, specimens M70 and M70HT show a relatively constant hardness profile, which does not include an abrupt drop in hardness.

Accordingly, with 70 % supported area, regardless of the type of support structures, enough heat could be dissipated from the system so that no heat source was created that would lower the hardness.

4. Conclusion

In this work, the influence of support structures in the Laser Powder Bed Fusion (L-PBF) process of AlSi10Mg on thermal conduction was investigated. The novelty of this study is the systematic variation of the supported sample area, which was investigated for two different types of support structures (columnar and meander). For this purpose, the supported area was varied from 10 to 70 % in 10 % steps for both support structure types. The component distortion, the microhardness profiles and the resulting microstructures were used as evaluation criteria for the influence on the resultant heat conduction. Each specimen type was examined in the as-built condition as well as after heat treatment (stress relieving). The following main conclusions can be drawn:

- Increasing the supported area has led to a reduction in distortion at the ends of the twin cantilever of up to about 30 % for both support structure types. Heat treatment, in form of stress relief annealing, has resulted in a significant distortion reduction of up to approximately 75 % for all supported surfaces for both support structure types.
- The increased supported area is accompanied by better heat dissipation. Consequently, fewer defects such as pores or dross defects occur, and a more homogeneous microstructure is formed at the transition from the support structures to the specimens. This is also reflected in more constant hardness profiles across the bar cross sections.
- The type of structure at the same percentage of supported area does not have a significant influence in the interval examined.
- Heat treatments significantly reduce distortion. When heat treatment is employed, the distortion is the same for any percentage of supported area.

In conclusion, the results show that, considering distortion, heat treatments should be employed. When, for any reason, heat treatments cannot be employed, a high percentage of supported area should be used. However, this also entails longer process times and longer times for post-processing, both increasing costs.

Acknowledgements

The authors would like to thank the EU European Regional Development Fund (ERDF) and the Ministry of Economics, Transport, Agriculture and Viticulture of the State of Rhineland-Palatinate for the financial support within the project “Center for Applied Additive Manufacturing with High-Speed Laser Directed Energy Deposition”.

*Naming of specific manufacturers is done solely for the sake of completeness and does not necessarily imply an endorsement of the named companies nor that the products are necessarily the best for the purpose.

References

[1] Künneke T, Zimmer D. Funktionsintegration additiv gefertigter Dämpfungsstrukturen bei Biegeschwingungen. In: Additive Fertigung von Bauteilen und Strukturen. Wiesbaden: Springer Vieweg; 2017: 61-74.
[2] Mertens AI, Delahaye J, Lecomte-Beckers J. Fusion-Based Additive Manufacturing for Processing Aluminum Alloys: State-of-the-Art and Challenges. Adv Eng Mater 2017; 19: 1700003.
[3] Mercelis P, Kruth J-P. Residual stresses in selective laser sintering and selective laser melting. Rapid Prototyp J 2006; 12: 254-265.
[4] Buchbinder D, Meiners W, Pirch N, Wissenbach K, Schrage J. Investigation on reducing distortion by preheating during manufacture of aluminum components using selective laser melting. J Laser Appl 2014; 26: 12004.
[5] Kruth J-P, Deckers J, Yasa E, Wauthlé R. Assessing and comparing influencing factors of residual stresses in selective laser melting using a novel analysis method. Proc Inst Mech Eng B: J Eng Manuf 2012; 226: 980-991.
[6] Buchbinder D, Schilling G, Meiners W, Pirch N, Wissenbach K. Untersuchung zur Reduzierung des Verzugs durch Vorwärmung bei der Herstellung von Aluminiumbauteilen mittels SLM. RTejournal 2011.
[7] Xu Y, Wang Z, Gong S, Chen Y. Reusable support for additive manufacturing. Addit Manuf 2021; 39: 101840.
[8] Leary M, Maconachie T, Sarker A, Faruque O, Brandt M. Mechanical and thermal characterisation of AlSi10Mg SLM block support structures. Mater Des 2019; 183: 108138.
[9] Xiaohui J, Chunbo Y, Honglan G, Shan G, Yong Z. Effect of supporting structure design on residual stresses in selective laser melting of AlSi10Mg. Int J Adv Manuf 2021; 118: 1597-1608.
[10] DIN EN ISO 6507-1: 2018-07, Metallische Werkstoffe - Härteprüfung nach Vickers - Teil 1: Prüfverfahren; Deutsche Fassung. Berlin: Beuth Verlag; 2018.
[11] Han Q, Gu H, Soe S, Setchi R, Lacan F, Hill J. Manufacturability of AlSi10Mg overhang structures fabricated by laser powder bed fusion. Mater Des 2018; 160: 1080-1095.
[12] Ullah R, Akmal J S, Laakso S V A, Niemi E. Anisotropy of additively manufactured AlSi10Mg: threads and surface integrity. Int J Adv Manuf 2020; 107: 3645-3662.
[13] Kempen K, Thijs L, van Humbeeck J, Kruth J-P. Processing AlSi10Mg by selective laser melting: parameter optimisation and material characterisation. Mater Sci Technol 2015; 31: 917-923.